Structural basis for discriminatory recognition of *Plasmodium* lactate dehydrogenase by a DNA aptamer

Yee-Wai Cheung[a], Jane Kwok[b], Alan W. L. Law[b], Rory M. Watt[c], Masayo Kotaka[b,1], and Julian A. Tanner[a,1]

Departments of [a]Biochemistry and [b]Physiology, Li Ka Shing Faculty of Medicine, and [c]Faculty of Dentistry, The University of Hong Kong, Pokfulam, Hong Kong Special Administrative Region, People's Republic of China

Edited by Dinshaw J. Patel, Memorial Sloan–Kettering Cancer Center, New York, NY, and approved August 14, 2013 (received for review May 20, 2013)

DNA aptamers have significant potential as diagnostic and therapeutic agents, but the paucity of DNA aptamer-target structures limits understanding of their molecular binding mechanisms. Here, we report a distorted hairpin structure of a DNA aptamer in complex with an important diagnostic target for malaria: *Plasmodium falciparum* lactate dehydrogenase (PfLDH). Aptamers selected from a DNA library were highly specific and discriminatory for *Plasmodium* as opposed to human lactate dehydrogenase because of a counterselection strategy used during selection. Isothermal titration calorimetry revealed aptamer binding to PfLDH with a dissociation constant of 42 nM and 2:1 protein:aptamer molar stoichiometry. Dissociation constants derived from electrophoretic mobility shift assays and surface plasmon resonance experiments were consistent. The aptamer:protein complex crystal structure was solved at 2.1-Å resolution, revealing two aptamers bind per PfLDH tetramer. The aptamers showed a unique distorted hairpin structure in complex with PfLDH, displaying a Watson–Crick base-paired stem together with two distinct loops each with one base flipped out by specific interactions with PfLDH. Aptamer binding specificity is dictated by extensive interactions of one of the aptamer loops with a PfLDH loop that is absent in human lactate dehydrogenase. We conjugated the aptamer to gold nanoparticles and demonstrated specificity of colorimetric detection of PfLDH over human lactate dehydrogenase. This unique distorted hairpin aptamer complex provides a perspective on aptamer-mediated molecular recognition and may guide rational design of better aptamers for malaria diagnostics.

SELEX | point-of-care diagnostics | X-ray crystallography | malaria diagnosis

Aptamers are artificially selected oligonucleotides that bind to molecular targets, typically proteins, with high specificity and avidity (1–3). DNA aptamers have been selected against dozens of targets for biomedical applications both as therapeutics (4, 5) and diagnostics (6, 7). Despite their widespread application, few DNA aptamer-target complex structures have been solved (8)–the best studied of which is the G-quadruplex aptamer that binds to thrombin (9–12). A DNA aptamer that binds to von Willebrand factor showed a three-stem structure of mainly B-form DNA with some noncanonical base pairing (13). Most recently, the structure of an innovative Slow Off-rate Modified Aptamer (SOMAmer) bound to platelet-derived growth factor B was solved, revealing binding via a hydrophobic surface that mimics how the factor binds to its receptor (14). Generally, the lack of DNA aptamer-target structures has limited our understanding of the mechanisms by which DNA aptamers attain their specificity (15), resulting in a bias in aptasensor development (16).

Better point-of-care tests are critically needed for malaria, a disease which continues to claim more than 1 million lives globally every year (17). Antimalarial drugs have been administered presumptively to patients with fever for decades, leading to drug resistance and poor management of other febrile illness. The cost of newer, more effective treatments has led to a situation whereby improved diagnostics has become a major factor that could reduce the burden of malaria in the developing world (17). Antibody-based rapid diagnostic tests have greatly benefitted malaria management, but significant issues with cost (17) and stability in tropical climates (18) remain that are intrinsically associated with the use of protein antibodies. DNA aptamers compare favorably to antibodies for diagnostic applications (19) with particular advantages that could be critical for diagnostic tests of the developing world: thermal stability, convenient chemical synthesis, and potentially lower costs of production (16). Here, we report the crystal structure and application of a unique DNA aptamer against an established malaria pan-species diagnostic target, *Plasmodium falciparum* lactate dehydrogenase (PfLDH) (20), and a mechanism of molecular recognition by a distorted hairpin DNA aptamer.

Results

Selected DNA Aptamers Show High Affinity and Specificity for PfLDH. PfLDH and two related human homologs human lactate dehydrogenase (hLDH) A1 and hLDHB were cloned, expressed in *Escherichia coli*, and purified (Fig. S1). DNA aptamers were selected from a library where each aptamer had a 35-base random region flanked by two constant primer-binding regions. Aptamers were selected by affinity chromatography to the target PfLDH immobilized on magnetic beads. To exclude nonspecific aptamers, selected aptamers were counterselected against the closely related human homologs hLDHA1 and hLDHB (Fig. S2). After 20 rounds of selection, 51 sequences were obtained and aligned, revealing the presence of conserved sequence signatures and motifs (Fig. S3).

Several selected aptamers were observed to specifically bind to PfLDH (the most promising with K_D in the range 20–50 nM)

Significance

Aptamers are oligonucleotides selected and evolved to bind tightly and specifically to molecular targets. Aptamers have promise as diagnostic tools and therapeutic agents, but little is known about how they recognize or discriminate their targets. In this study, X-ray crystallography together with several other biophysical techniques reveal how a new DNA aptamer recognizes and discriminates *Plasmodium* lactate dehydrogenase, a protein marker that is a diagnostic indicator of infection with the malaria parasite. We also demonstrate application of the aptamer in target detection. This study broadens our understanding of aptamer-mediated molecular recognition and provides a DNA aptamer that could underpin new innovative approaches for point-of-care malaria diagnosis.

Author contributions: Y.-W.C., R.M.W., M.K., and J.A.T. designed research; Y.-W.C., J.K., A.W.L.L., and M.K. performed research; Y.-W.C., M.K., and J.A.T. analyzed data; and Y.-W.C., R.M.W., M.K., and J.A.T. wrote the paper.

The authors declare no conflict of interest.

This article is a PNAS Direct Submission.

Data deposition: The atomic coordinates and structure factors have been deposited in the Protein Data Bank, www.pdb.org (PDB ID code 3ZH2).

[1]To whom correspondence may be addressed. E-mail: jatanner@hku.hk or masayo@hku.hk.

This article contains supporting information online at www.pnas.org/lookup/suppl/doi:10.1073/pnas.1309538110/-/DCSupplemental.

without observable binding to hLDHA1 and hLDHB by isothermal titration calorimetry (ITC) (Fig. 1*C* and Table S1), electrophoretic mobility shift assay (EMSA) (Fig. S4), and surface plasmon resonance (SPR) spectroscopy (Fig. S5). A single DNA aptamer that showed significant promise (2008s) in the three binding assays (with sequence shown in Fig. 1*B*) was taken forward for structural analysis. This aptamer showed a K_D for PfLDH of 42 nM by ITC for the interaction in solution and a stoichiometry that would imply 2:1 protein:aptamer molar ratio of binding if considering protomer molar concentration of PfLDH (Fig. 1*C*). Surface plasmon resonance was performed by immobilizing the PfLDH to a Ni-NTA sensor chip surface and injecting different concentrations of 2008s aptamer over the surface. A heterogeneous ligand model fitted the sensorgrams

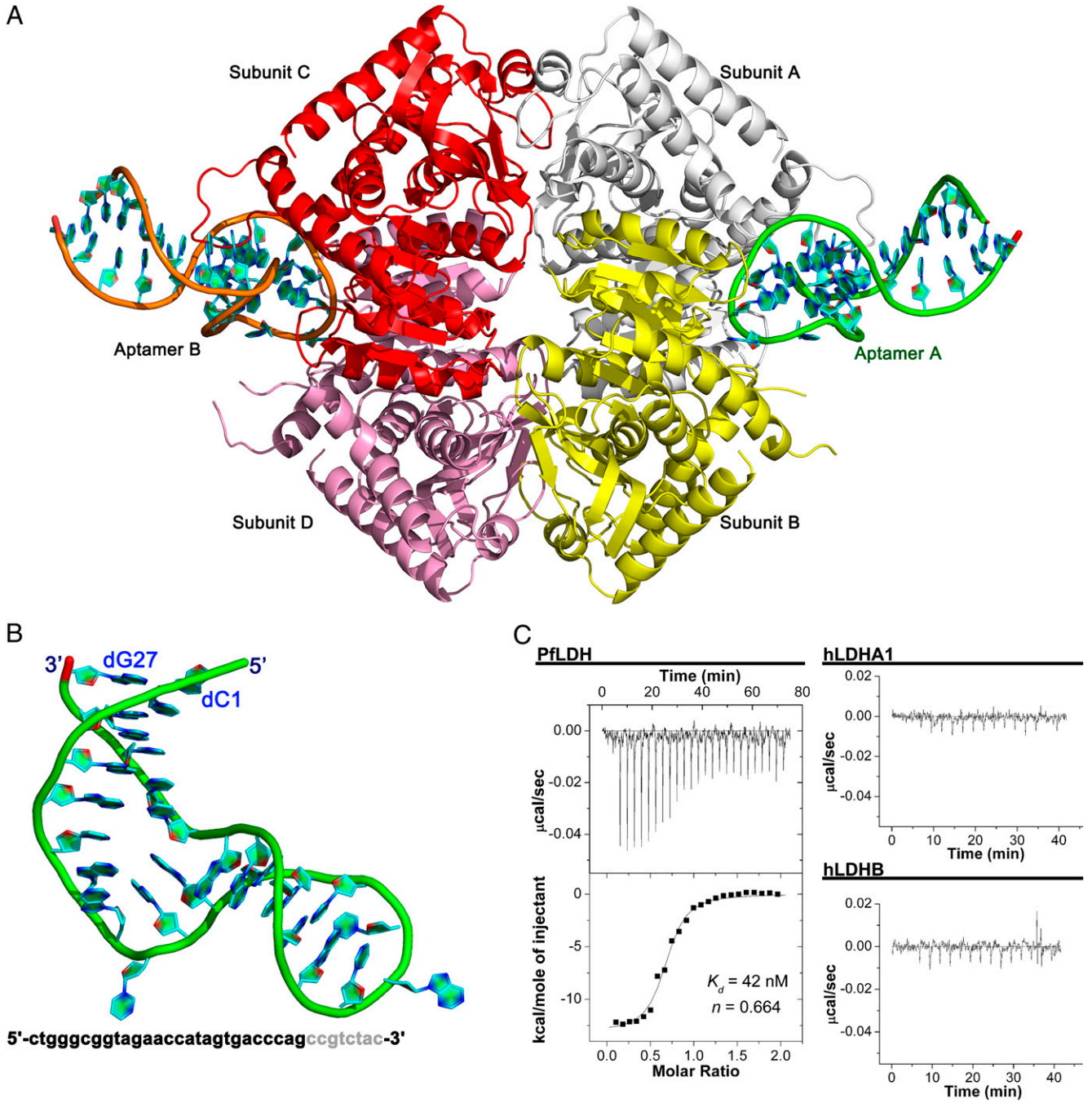

Fig. 1. The tetrameric PfLDH binds two DNA aptamers. (*A*) Crystal structure of tetrameric PfLDH in complex with two 2008s DNA aptamers. The A, B, C, and D subunits of PfLDH are colored in white, yellow, red, and pink, respectively. One 2008s aptamer (designated aptamer A) spans subunits A and B, whereas the other 2008s aptamer (designated aptamer B) spans subunits C and D. (*B*) Structure and sequence of the 2008s DNA aptamer alone in the complexed state. The 2008s aptamer shows a distorted hairpin comprising a B-helical stem, an asymmetric internal loop containing flipped base T^9, and an apical loop containing flipped base A^{16}. Clear electron density was observed in the crystal structure for the first 27 bases of each aptamer (colored in black in sequence), and no electron density was observed for the last eight bases at the 3′ of each aptamer (colored in gray in sequence). (*C*) Isothermal titration calorimetry titrations for 2008s aptamer binding to PfLDH (*Left*) and human LDHA1 and LDHB (*Right*). Data were fitted to a single-site model revealing K_D = 42 nM and approximate 2:1 protein subunit:aptamer molar stoichiometry (*Lower Left*).

(Fig. S5) revealing a tight binding site (apparent K_D^1 = 59 nM) consistent with the ITC data, and association rates and dissociation rates typical of DNA–protein interactions ($k_a^1 = 2.8 \times 10^6$ $M^{-1}{\cdot}s^{-1}$ and $k_d^1 = 0.16\ s^{-1}$) (Table S2). A further apparent weaker site (apparent K_D^2 = 968 nM) was observed, which we discuss below in light of the structural data obtained. Data from EMSAs performed to visualize the interaction between 2008s and PfLDH yielded a K_D of 56 ± 18 nM (Fig. S4) and indicated a complete absence of observable binding of 2008s to either human lactate dehydrogenase (LDH) protein at concentrations up to at least 5.7 μM (Fig. S4). Thus, results from three independent biophysical techniques were in good agreement that PfLDH bound the 2008s aptamer tightly and specifically with a dissociation constant in the range 42–59 nM.

X-Ray Complex Crystal Structure Reveals Two Aptamers Bind per Tetrameric PfLDH with a Unique Distorted Hairpin Structure. We determined the crystal structure of the PfLDH–aptamer complex by X-ray crystallography at 2.1 Å resolution (Fig. 1*A*, Fig. S6, and Table S3). The four subunits of PfLDH in the asymmetric unit are organized into a tetramer with characteristic 222 symmetry, similar to previously determined PfLDH X-ray crystallographic structures (21, 22). Each of the two single-stranded DNA aptamers were seen bound to the Q-axis dimers formed by subunits A and B (or subunits C and D), spanning the large cofactor domains of the two juxtaposed monomers.

The aptamers showed a distorted hairpin structure in complex with PfLDH (Fig. 1*B*). Clear electron density was observed for the first 27 bases of both aptamers in the asymmetric unit; no electron density was observed beyond the hairpin structure for the last eight bases at the 3′ end of the aptamer, probably because the aptamer tail is disordered. The global fold of the aptamer adopted a distorted hairpin structure with a $C^{15}A^{16}T^{17}A^{18}$ apical tetraloop, an asymmetric internal loop with six bases in one strand ($C^6G^7G^8T^9A^{10}G^{11}$) and one base in the other (A^{22}), and a terminal B-form helix. The aptamer contains seven Watson–Crick type base pairs, five of which form the terminal B-form helical stem DNA duplex. The remaining two Watson–Crick type base pairs, together with noncanonical base pairing between A^{12} and G^{21}, form the DNA duplex flanking between the internal loop and apical loop. Similar to the terminal B-helical stem, this short duplex assumes B-helical geometry. The two B-helices are oriented in a ∼140° angle, resulting in an overall bent shape for the DNA aptamer. C^6 of the internal loop is involved in a stacking interaction with its neighbor, G^5 of the stem B helix. As a result, C^6, G^7, and G^8 of the internal loop remain within the stem B helix as they continuously stack. G^7 and A^{10} form a noncanonical base pair in the internal loop. T^9 is flipped out of the internal loop and is engaged in aptamer–PfLDH interactions as described below. In the apical tetraloop, both T^{17} and A^{18} are involved in stacking interactions and remain in the helical axis of the short duplex flanking the apical loop and internal loop. C^{15} and A^{16} are flipped out of the apical loop; the position of C^{15} is stabilized by interaction of N4 with the backbone phosphate of C^{14}, whereas A^{16} is involved in indirect interactions with PfLDH via water molecules.

Nature of Aptamer Binding to PfLDH. Each aptamer interacts through extensive salt bridges with the cofactor binding sites of two PfLDH subunits of the Q-axis dimer, composed of subunits A and B or C and D (Fig. 2*A*). The interface between the aptamer and PfLDH buries a solvent-accessible surface of 1,276 $Å^2$ on each aptamer and 895 $Å^2$ and 394 $Å^2$ for subunits A/C and B/D of PfLDH, respectively. The aptamer interacts with the substrate specificity loop at the tip of the cofactor binding sites of the two adjacent PfLDH subunits via distinct regions. Subunit A/C interacts with the internal loop, whereas subunit B/D interacts with the apical tetraloop. Such asymmetry may explain the apparent strong and weak binding sites observed by the SPR biosensor experiments in Fig. S5. Such SPR responses may be explained by distinct encounter (with subunit A/C) and docking (with subunit B/D) two-phase association and dissociation events (23).

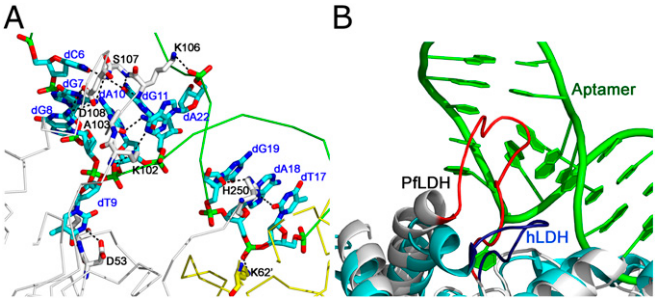

Fig. 2. The substrate specificity loop at the protein:aptamer binding interface determines the discrimination of the aptamer for PfLDH over human LDH. (*A*) Direct interactions of the 2008s DNA aptamer with PfLDH. Extensive interactions are observed between bases 6–11 and base 22 of the 2008s aptamer with the substrate specificity loop in subunit A/C (colored in white), and less extensive interactions are observed between bases 17 and 19 and subunit B/D (colored in yellow). Each aptamer buries 895 Å on subunit A/C and buries 394 Å on subunit B/D. (*B*) Discrimination of aptamer specificity in binding to PfLDH over hLDH is explained by differences in the substrate specificity loop. The substrate specificity loops of PfLDH and hLDHB are colored red and blue, respectively.

The bases C^6, G^7, G^8, G^{11}, and A^{22} of the internal loop of the DNA aptamer, which interacts with subunits A/C of PfLDH, form extensive base interactions with residues 102A-108A of the PfLDH extended substrate specificity loop. Backbone interactions are also seen with Lys102A and Lys106A forming contacts with the phosphates of A^{10} and A^{22}, respectively. The flipped base T^9 extends away from the bent hairpin structure into the adenine end of the NADH binding cleft and is stabilized by hydrogen bonds between N3 of the T^9 base and the side chain of Asp53A, and O4 of the T^9 base with the amino nitrogen of Ile54A.

Compared with the interaction of the internal loop and subunit A/C of PfLDH, the interaction of the apical tetraloop with subunit B/D of PfLDH is less extensive and involves indirect contacts via water molecules. Direct backbone contacts are observed with phosphate groups of A^{18} and G^{19} of the tetraloop interacting with the side chains of Lys62B and His250B of the NADH binding cleft. Similar to T^9 in the internal loop, the flipped base A^{16} extends into the adenine end of the NADH binding cleft of subunit B/D. However, instead of forming direct interactions with the protein, the position of A^{16} of the apical loop is stabilized via indirect interactions with the protein via water molecules (Fig. 2*A*).

Superposition of Human LDHB Structure Reveals an Extended Substrate Specificity Loop That Dictates Aptamer Specificity. The extensive interaction of the aptamer to the unique extended substrate specificity loop of PfLDH (amino acids 102–108) contributes to the high specificity of aptamer binding to PfLDH versus human LDH. Indeed, superposition of human LDHB (PDB ID code: 1T2F; ref. 24) with our PfLDH–aptamer structure revealed that human LDH lacks the extension at the substrate specificity loop, resulting in an inability to reach the aptamer (Fig. 2*B*). Thus, binding of the aptamer to human LDH would not occur, which both proves that the counter selection strategy was successful and provides a structural explanation for the specificities determined in our binding assays.

Relation of Aptamer Binding to Substrate and Cofactor Binding. The 2008s aptamer did not inhibit the enzymatic activity of PfLDH nor of human LDH controls (Fig. S7). To understand this absence of inhibitory activity, we superimposed our structure of the aptamer–PfLDH complex with the previously solved PfLDH

structure in complex with substrate analogs, NAD^+ and oxamate (PDB ID code: 1LDG; ref. 21) (Fig. 3*A*). We observed at the global level that the aptamer binds at a site distinct from the substrate binding sites, but close to the cofactor binding sites (Fig. 3*A*). In the substrate-complexed structure, the substrate specificity loop closes on top of the substrates holding them in place (Fig. 3*B*). In the previous section, we mentioned how the binding of the aptamer to PfLDH may block the binding of the adenine end of the cofactor NADH. However, by holding the substrate specificity loop in an open conformation, NADH may still enter the active site in a different conformation, thereby explaining the absence of inhibitory activity of the aptamer despite tight binding to the enzyme (Fig. 3*C*).

Conjugation of Aptamers to Gold Nanoparticles Provides a Colorimetric Assay for PfLDH and Further Demonstrates Specificity of Binding. The PfLDH aptamer was conjugated to gold nanoparticles (AuNPs) to develop a colorimetric assay for PfLDH (Fig. 4*A*) (25). Transmission electron microscopy revealed that the AuNP aggregated specifically in the presence of PfLDH (Fig. 4*B*). The red color (absorbance peak of 520 nm; Fig. S8) was specifically lost in the presence of 25 ng/μL PfLDH but not in the presence of hLDHA1, hLDHB, or other controls (Fig. 4 *C* and *D*). The limit of detection was determined by using the statistically estimated limit of the blank to be 57 pg/μL PfLDH (Fig. S9). This limit of detection is a promising starting point with regards to future clinical diagnostic applications because patients infected with PfLDH typically show PfLDH plasma levels around 3–15 pg/μL plasma (26), which can easily be concentrated to a range within the limit of detection against a typical background human LDH level of 100–400 pg/μL. Therefore, discrimination by the 2008s aptamer would be sufficient, and the sensitivity should be attainable with further development. Overall, our experiments establish that the DNA aptamer identified can specifically recognize PfLDH because of its unique loop that is not present in human LDH and demonstrate a proof of principle for downstream malaria diagnostic development.

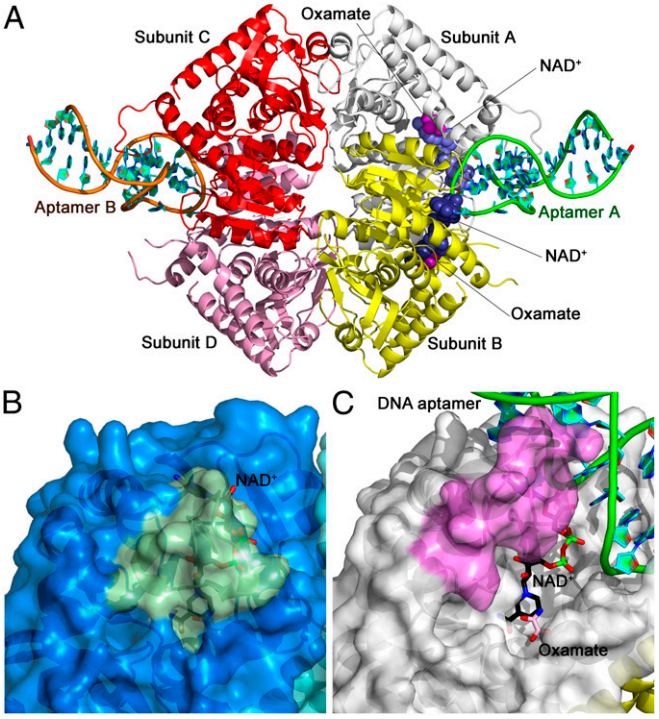

Fig. 3. Visualization of aptamer and substrate binding sites on PfLDH. (*A*) Substrate-bound PfLDH (PDB ID code: 1LDG; ref. 21) was superposed onto subunits A and B of aptamer-bound PfLDH tetramer. For clarity, only the superposed oxamate (in dark pink and magenta) and NAD^+ (in slate and dark blue) from substrate-bound PfLDH were shown as space-filled models. (*B*) As seen from the structure of the substrate-bound PfLDH, when substrate and cofactor are bound, the substrate-specificity loop of PfLDH (shown in pale green) closes over the active site covering the bound substrate and cofactor. (*C*) When 2008s DNA aptamer is bound to PfLDH, the substrate-specificity loop (shown in pink) is held by the aptamer in an open conformation, exposing the active site. Only the superposed oxamate and NAD^+ from the substrate-bound PfLDH are shown as ball-and-stick models for clarity.

Discussion

The challenges surrounding the solution of crystal structures of aptamer–protein complexes were reviewed (8). Although a number of RNA aptamer/protein complex structures have been solved, only the thrombin–aptamer (9–12) and Von Willebrand Factor–aptamer complexes (13) have been solved for a DNA aptamer. Furthermore, a SOMAmer incorporating synthetic nucleotide modifications complex structure was solved with its target platelet-derived growth factor B (14). The distorted hairpin structure reported herein is quite distinct from the G-quadruplex aptamer that binds to thrombin (9–12), the B-DNA aptamer that binds to von Willebrand factor (13), and the SOMAmer that exhibits a hydrophobic binding interface (14). The SOMAmers showed very low dissociation constants in the picomolar range, principally due to their far slower dissociation rates (14). As a counterpoint to these three other structures, this study broadens our understanding of how DNA aptamers specifically recognize and bind to their targets.

A group recently published a pair of papers identifying aptamers against PfLDH (27) and against *Plasmodium vivax* LDH (28). Their aptamers were distinct from those presented here, yet sequence homology shows they may share some structural similarities with a likely stem loop, although they did not investigate the structure of their aptamers (27). Dissociation constants for the interaction with PfLDH were in a similar range (16.8–49.6 nM) to those we observe here. Using an aptasensor linked to an electrochemical impedance spectroscopy assay they could demonstrate a detection limit of 1 pM (27), and detected both *P. vivax* and *Plasmodium falciparum* at less than 100 parasites per microliter. The combination of their results, together with the structural insight we provide herein, provides a strong argument that aptamer-mediated molecular recognition could have potential for the diagnosis of malaria.

In particular, the structure provides a guide for possible modifications to the aptamer by rational design. For example, the final eight bases of the aptamer which were observed to be disordered may be unnecessary in a potential diagnostic. The base pair loop that is critical to aptamer folding but is not involved directly at the binding interface also provides a clear mechanism by which to link the aptamer to a solid support or within more elaborate diagnostic modalities. Stabilization, extension, or inclusion of modified bases within the stem loop could decrease the dissociation constants or dissociation rates of the 2008s aptamer. The innovative SOMAmer technology has demonstrated the importance of slow dissociation rates (off rates) for aptamers (14) and, thus, specific tailoring to slow dissociation rate could be one promising approach. Aptamers could be incorporated into a variety of visualizable assays including aptamer-based lateral flow dipstick tests (29), cross-linked hydrogels (30), aptamer-based origami paper (31), or other emerging technologies (7, 32).

In conclusion, we present the identification, structural characterization, and application of a distorted hairpin DNA aptamer against PfLDH. Notably, we demonstrate that specificity of the DNA aptamer is achieved by discriminatory binding to a loop that is present only in the *Plasmodium* but not in the human lactate dehydrogenase, visualizing the evolutionary outcome of a Systematic Evolution of Ligands by Exponential Enrichment

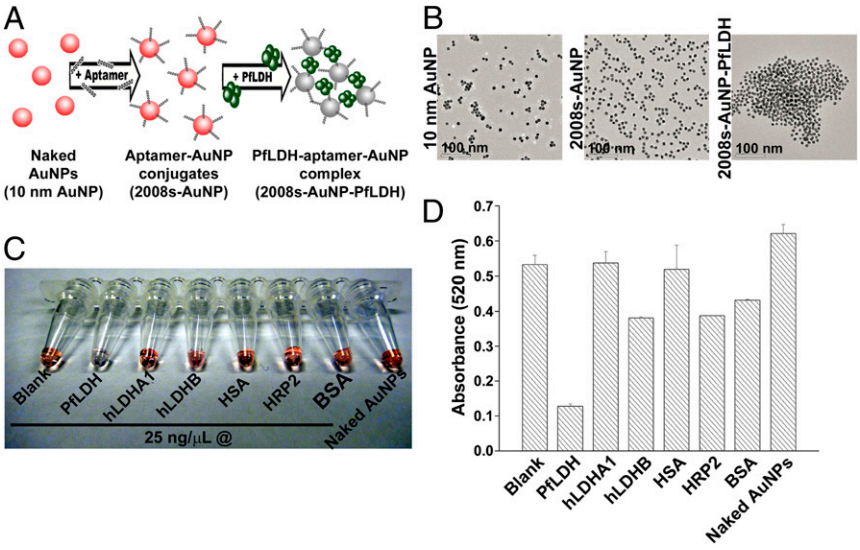

Fig. 4. Aptamers conjugated to gold nanoparticles to demonstrate potential for application. (*A*) Principle of approach. (*B*) Transmission electron microscopy images of nonconjugated gold nanoparticles (*Left*), aptamer-conjugated gold nanoparticles (*Center*), and aptamer-conjugated gold nanoparticles in presence of PfLDH (*Right*). (*C*) Qualitative observation using gold nanoparticles to detect PfLDH specifically at 25 ng/μL. (*D*) Quantitative absorbance of data in *C*.

(SELEX) process that includes negative counterselection steps. The widely investigated anticoagulant thrombin aptamer (9, 10) acted as a foundation for dozens of investigations where the innovation lay in the detection method rather than the aptamer and its clinically relevant target—the aptly named "thrombin problem" (16). This insight into how an aptamer specifically recognizes and discriminates PfLDH broadens our understanding of aptamer-mediated molecular recognition and may be important in the development of innovative approaches critically needed for point-of-care malaria diagnosis.

Materials and Methods

Cloning, Expression, and Purification of PfLDH and Human Lactate Dehydrogenases hLDHA1 and hLDHB. The *PfLDH* ORF was amplified by PfLDH-S, ATTATTGCTAGCATGGCACCAAAAGCAAAAATCGTTTTAGTTG and PfLDH-AS, ATTATTCTCGAGTTAAGCTAATGCCTTCATTCTCTTAGTTTCA, using a *P. falciparum* 3D7 cDNA library as a template, followed by ligation into the NcoI/XhoI-digested pET-28a (Novagen) vector (underline indicates start codon). The *hLDHA1* ORF was amplified by hLDHA1-S ATTATTGAATTCATGGCAACTCTAAAGGATCAGC-TGA, and hLDHA1-AS, ATTATTAAGCTTTTAAAATTGCAGCTCCTTTTGGATC, using cDNA extracted from human liver tissue as a template, followed by ligation into the NheI/HindIII-digested pET-28a (Novagen) vector. ORF of *hLDHB* was amplified by hLDHB-S, ATTATTGCTAGCATGGCAACTCTTAAGGAAAAACTCATTG-CACC and hLDHB-AS, ATTATTGCGGCCGCTCACAGGTCTTTTAGGTCCTTCTGG, using cDNA extracted from human liver tissue as a template, followed by ligation into the NheI/NotI-digested pET-28a (Novagen) vector. The plasmids were transformed into *E. coli* BL21 (DE3) pLysS for isopropyl β-D-1-thiogalactopyranoside (IPTG)-induced expression. Bacterial culture was incubated at 37 °C until OD_{600} = 0.5, then 0.5 mM IPTG was added followed by 4-h expression at 25 °C. Pellets were collected, sonicated, and expressed proteins were purified by using HisTrap chromatography (GE Healthcare).

In Vitro Selection of DNA Aptamers. A single-stranded DNA (ssDNA) library containing a 35-mer random region flanked by two 18-mer priming regions (5′–CGTACGGTCGACGCTAGC-[N35]-CACGTGGAGCTCGGATCC–3′) was used as starting material for in vitro selection. Two namomoles of ssDNA library was incubated with 1 nmol of target protein that was conjugated with Ni-NTA magnetic beads. The unbound species were removed, and the ssDNA-protein-magnetic beads complexes were suspended in 10 μL of water for PCR amplification of PfLDH-bound species by using forward primer (5′–CGTACGGTCGACGCTAGC–3′) and reverse primer with biotinylated 5′ end (5′–biotin–GGATCCGAGCTCCACGTG–3′) using Pwo SuperYield DNA polymerase (Roche). PCR conditions were as follows: denaturation at 95 °C for 15 s, annealing at 50 °C for 30 s and elongation at 72 °C for 15 s for 10 cycles. Enriched DNA aptamer pool was purified by streptavidin magnetic beads followed by a wash of 100 mM NaOH to remove the nonbiotinylated complementary strand. The resultant ssDNA pool was used for the next round of selection. Counterselections by using Ni-NTA magnetic agarose beads (after rounds 4 and 7), hLDHA1-immobilized Ni-NTA magnetic agarose beads (after rounds 6 and 10), and hLDHB-immobilized Ni-NTA magnetic agarose beads (after rounds 5 and 9) were incorporated in between the SELEX cycles.

Crystallization and Structure Solution. The complex between PfLDH and the DNA aptamer was formed by mixing protein and DNA in a 1:1 molar ratio for crystallization. Screening of crystallization conditions was performed by using Mosquito liquid handler (TTP Labtech) at 291 K using the sitting-drop vapor diffusion method by mixing 100 nL of protein:DNA complex with an equal volume of crystallization solution. Of the 576 conditions screened, several hits for protein:DNA complex were observed. The best crystals were obtained under condition 26 of the Hampton Research Matrix Screen (0.2 M KCl, 0.1 M magnesium acetate, 0.05 M sodium cacodylate at pH 6.5, and 10% (wt/vol) PEG 8000).

The crystal of PfLDH–aptamer complex was cryoprotected in a solution of 30% (vol/vol) glycerol mixed with the reservoir solution. Data were collected at beamline 13B1, National Synchrotron Radiation Research Center, Taiwan. Data were indexed and integrated with HKL2000 (33). The structure was solved by molecular replacement using the program PHASER (34) with the structure of LDH (PDB ID code: 1LDG) (21). The structure of the DNA aptamer was built manually with COOT (35), and the complex structure was refined in REFMAC (36).

ITC. For ITC, PfLDH aptamers and PfLDH were dialyzed in 25 mM Tris·HCl at pH 7.5 containing 0.1 M NaCl and 20 mM imidazole. All of the buffers, protein, and aptamers were degassed for 10 min at 25 °C before ITC experiments. All of the experiments were performed in 25 mM Tris·HCl at pH 7.5 containing 0.1 M NaCl and 20 mM imidazole at 25 °C by using iTC_{200} microcalorimeter (MicroCal). ITC experiments were carried out by injecting PfLDH aptamer (typically 20 μM) into buffered PfLDH (typically 7.69 μM) solutions. The ITC data were analyzed by using Origin v7.0 software (MicroCal) to integrate the titration curves for extracting the thermodynamic parameters, stoichiometry (N), equilibrium association constant [$K_A = (K_D)^{-1}$)], and the binding enthalpy (ΔH).

EMSAs. EMSAs were carried out by incubating 25 nM PfLDH aptamer 2008s with different proteins at concentrations ranging from 0 to 5.7 μM (concentration of tetramer) in 25 mM Tris·HCl at pH 7.5 containing 0.1 M NaCl and 20 mM imidazole at room temperature for 1 h. Reactions were loaded on 12% native polyacrylamide gels and visualized by SYBR gold nucleic acid gel staining (Invitrogen). Data were fit to a logistic equation.

SPR. SPR measurements were performed by using a Biacore X100 instrument (GE Healthcare). PfLDH was immobilized on the surface of a NTA sensor chip (GE Healthcare). A running buffer containing 25 mM Tris·HCl at pH 7.5, 100 mM NaCl, 20 mM imidazole, and 0.005% (vol/vol) P20 was used for ligand capture. Flow cell 2 was charged by using 500 μM $NiSO_4$, then purified PfLDH was immobilized on the surface to a density of ~2,000 response units by a 60-s injection followed by 300-s stabilization. Flow cell 1 was unmodified as control reference. Different concentrations of 2008s aptamer (12.5, 25, 50,

100, 200, and 350 nM) were prepared in identical buffer and injected for 60 s at 30 μL/min followed by a 120-s stabilization. Every injection was performed in triplicate with full regeneration of surface between runs. Initial fitting was by the Biacore X100 Plus Package software before export to Origin v8.5 (OriginLab). As a single-site model did not appropriately describe the interaction, data were fit to a heterogeneous ligand model. Dissociation was fitted to the following equation:

$$R_t = R_0 e^{-k_d^1 \cdot t} + R_0 e^{-k_d^2 \cdot t}$$

where R_t is the measured response at time t after start of dissociation, R_0 is the measured response at start of dissociation, t is the time in seconds after start of dissociation, and k_d^1 and k_d^2 are the dissociation rate constants for the first and second interactions.

Association was fitted to the following equation:

$$R_t = \left(\frac{k_a^1 c R_{max}^1}{k_a^1 c + k_d^1}\right) \cdot \left(1 - e^{-\left(k_a^1 c + k_d^1\right)t}\right) + \left(\frac{k_a^2 c R_{max}^2}{k_a^2 c + k_d^2}\right) \cdot \left(1 - e^{-\left(k_a^2 c + k_d^2\right)t}\right)$$

where R_t is the measured response at time t after start of association, R_{max}^1 and R_{max}^2 are the maximal responses for the first and second interactions, t is the time in seconds after start of association, c is the concentration of aptamer, and k_a^1, k_d^1, k_a^2, and k_d^2 are the respective association and dissociation rate constants for the first and second interactions.

Assay for LDH Enzyme Activity. A previously described assay (37) for reduction of pyruvate to L-lactate catalyzed by LDH was performed under multiple concentrations of 2008s aptamer. LDH activity was assayed in 25 mM Tris·HCl at pH 7.5, 5 mM pyruvate, 1 mM NADH, and change in absorbance was measured at 340 nm at 25 °C to reflect oxidation of NADH to NAD^+.

Preparation of Aptamer-Immobilized Gold Nanoparticles. The PfLDH aptamer, 2008s, was conjugated to 10-nm gold colloid (gold nanoparticles, AuNP) (Sigma) via a 5′ thiol group according to the protocol described by Taton (38) with modifications. All of the incubations were carried at room temperature in the dark. Disulfide-functionalized aptamer was reduced by 0.1 M DTT for 30 min at room temperature before use. The reduced aptamers were purified by using Sephadex G-25 (Pharmacia Biotech). Reduced aptamers (2.5 nmol) were then added to 500 μL of AuNP. After 24 h of incubation, 1 M NaCl and 0.1 M sodium phosphate buffer were added to reach final concentrations of 0.1 M NaCl and 10 mM phosphate buffer, respectively. The aptamer/gold nanoparticle mixture was aged at room temperature for another 24 h. 2008s–AuNP was separated from the solution by centrifugation followed by washing in 0.1 M NaCl/10 mM sodium phosphate buffer at pH 7. A 37-mer of polythymine (polyT) was conjugated to AuNP by the above procedures for use in control experiments. The aptamer–AuNP conjugates were stored in 0.3 M NaCl/0.01% sodium azide/10 mM sodium phosphate buffer at pH 7.0.

Characterization of 2008s–AuNP. ***UV-Vis spectrometry.*** The spectrometry analyses were carried out by using a Varioskan Flash Multimode Reader (Thermo Scientific). The spectrum was derived from at least three experiments.

Transmission electron microscopy. Oligonucleotides (aptamers) immobilized on AuNPs were characterized by using a Philips CM100 transmission electron microscopy. Approximately 10 μL of aptamer–AuNP conjugates were coated on a 200 mesh copper grid by adding sample to the grid and dried at room temperature.

ACKNOWLEDGMENTS. We thank the staff of beamline 13B1 of the National Synchrotron Radiation Research Center (Taiwan) for their help. This work was supported by the Hong Kong University Grants Council under General Research Fund Grant HKU776108M (to J.A.T.).

1. Ellington AD, Szostak JW (1990) In vitro selection of RNA molecules that bind specific ligands. *Nature* 346(6287):818–822.
2. Ellington AD, Szostak JW (1992) Selection in vitro of single-stranded DNA molecules that fold into specific ligand-binding structures. *Nature* 355(6363):850–852.
3. Tuerk C, Gold L (1990) Systematic evolution of ligands by exponential enrichment: RNA ligands to bacteriophage T4 DNA polymerase. *Science* 249(4968):505–510.
4. Bunka DHJ, Platonova O, Stockley PG (2010) Development of aptamer therapeutics. *Curr Opin Pharmacol* 10(5):557–562.
5. Keefe AD, Pai S, Ellington A (2010) Aptamers as therapeutics. *Nat Rev Drug Discov* 9(7):537–550.
6. Cass AE, Zhang Y (2011) Nucleic acid aptamers: Ideal reagents for point-of-care diagnostics? *Faraday Discuss* 149:49–61, discussion 63–77.
7. Famulok M, Mayer G (2011) Aptamer modules as sensors and detectors. *Acc Chem Res* 44(12):1349–1358.
8. Ruigrok VJ, et al. (2012) Characterization of aptamer-protein complexes by x-ray crystallography and alternative approaches. *Int J Mol Sci* 13(8):10537–10552.
9. Griffin LC, Tidmarsh GF, Bock LC, Toole JJ, Leung LL (1993) In vivo anticoagulant properties of a novel nucleotide-based thrombin inhibitor and demonstration of regional anticoagulation in extracorporeal circuits. *Blood* 81(12):3271–3276.
10. Padmanabhan K, Padmanabhan KP, Ferrara JD, Sadler JE, Tulinsky A (1993) The structure of alpha-thrombin inhibited by a 15-mer single-stranded DNA aptamer. *J Biol Chem* 268(24):17651–17654.
11. Russo Krauss I, et al. (2011) Thrombin-aptamer recognition: A revealed ambiguity. *Nucleic Acids Res* 39(17):7858–7867.
12. Russo Krauss I, et al. (2012) High-resolution structures of two complexes between thrombin and thrombin-binding aptamer shed light on the role of cations in the aptamer inhibitory activity. *Nucleic Acids Res* 40(16):8119–8128.
13. Huang RH, Fremont DH, Diener JL, Schaub RG, Sadler JE (2009) A structural explanation for the antithrombotic activity of ARC1172, a DNA aptamer that binds von Willebrand factor domain A1. *Structure* 17(11):1476–1484.
14. Davies DR, et al. (2012) Unique motifs and hydrophobic interactions shape the binding of modified DNA ligands to protein targets. *Proc Natl Acad Sci USA* 109(49): 19971–19976.
15. Tucker WO, Shum KT, Tanner JA (2012) G-quadruplex DNA aptamers and their ligands: Structure, function and application. *Curr Pharm Des* 18(14):2014–2026.
16. Baird GS (2010) Where are all the aptamers? *Am J Clin Pathol* 134(4):529–531.
17. Rafael ME, et al. (2006) Reducing the burden of childhood malaria in Africa: The role of improved. *Nature* 444(Suppl 1):39–48.
18. Jorgensen P, Chanthap L, Rebueno A, Tsuyuoka R, Bell D (2006) Malaria rapid diagnostic tests in tropical climates: The need for a cool chain. *Am J Trop Med Hyg* 74(5):750–754.
19. Cho EJ, Lee JW, Ellington AD (2009) Applications of aptamers as sensors. *Annu Rev Anal Chem (Palo Alto Calif)* 2:241–264.
20. Wilson ML (2012) Malaria rapid diagnostic tests. *Clin Infect Dis* 54(11):1637–1641.
21. Dunn CR, et al. (1996) The structure of lactate dehydrogenase from Plasmodium falciparum reveals a new target for anti-malarial design. *Nat Struct Biol* 3(11): 912–915.
22. Read JA, Wilkinson KW, Tranter R, Sessions RB, Brady RL (1999) Chloroquine binds in the cofactor binding site of Plasmodium falciparum lactate dehydrogenase. *J Biol Chem* 274(15):10213–10218.
23. Lipschultz CA, Li Y, Smith-Gill S (2000) Experimental design for analysis of complex kinetics using surface plasmon resonance. *Methods* 20(3):310–318.
24. Cameron A, et al. (2004) Identification and activity of a series of azole-based compounds with lactate dehydrogenase-directed anti-malarial activity. *J Biol Chem* 279(30):31429–31439.
25. Liu JW, Lu Y (2005) Fast colorimetric sensing of adenosine and cocaine based on a general sensor design involving aptamers and nanoparticles. *Angew Chem Int Ed Engl* 45(1):90–94.
26. Martin SK, Rajasekariah GH, Awinda G, Waitumbi J, Kifude C (2009) Unified parasite lactate dehydrogenase and histidine-rich protein ELISA for quantification of Plasmodium falciparum. *Am J Trop Med Hyg* 80(4):516–522.
27. Lee S, et al. (2012) A highly sensitive aptasensor towards Plasmodium lactate dehydrogenase for the diagnosis of malaria. *Biosens Bioelectron* 35(1):291–296.
28. Jeon W, Lee S, Manjunatha DH, Ban C (2013) A colorimetric aptasensor for the diagnosis of malaria based on cationic polymers and gold nanoparticles. *Anal Biochem* 439(1):11–16.
29. Liu JW, Mazumdar D, Lu Y (2006) A simple and sensitive "dipstick" test in serum based on lateral flow separation of aptamer-linked nanostructures. *Angew Chem Int Ed Engl* 45(47):7955–7959.
30. Zhu Z, et al. (2010) An aptamer cross-linked hydrogel as a colorimetric platform for visual detection. *Angew Chem Int Ed Engl* 49(6):1052–1056.
31. Liu H, Xiang Y, Lu Y, Crooks RM (2012) Aptamer-based origami paper analytical device for electrochemical detection of adenosine. *Angew Chem Int Ed Engl* 51(28): 6925–6928.
32. Mayer G (2009) The chemical biology of aptamers. *Angew Chem Int Ed Engl* 48(15): 2672–2689.
33. Minor W, Tomchick D, Otwinowski Z (2000) Strategies for macromolecular synchrotron crystallography. *Structure* 8(5):R105–R110.
34. McCoy AJ (2007) Solving structures of protein complexes by molecular replacement with Phaser. *Acta Crystallogr D Biol Crystallogr* 63(Pt 1):32–41.
35. Emsley P, Cowtan K (2004) Coot: Model-building tools for molecular graphics. *Acta Crystallogr D Biol Crystallogr* 60(Pt 12 Pt 1):2126–2132.
36. Winn MD, Murshudov GN, Papiz MZ (2003) Macromolecular TLS refinement in REFMAC at moderate resolutions. *Methods Enzymol* 374:300–321.
37. Berwal R, Gopalan N, Chandel K, Prasad GB, Prakash S (2008) Plasmodium falciparum: Enhanced soluble expression, purification and biochemical characterization of lactate dehydrogenase. *Exp Parasitol* 120(2):135–141.
38. Taton TA (2002) Preparation of gold nanoparticle-DNA conjugates. *Current Protoc Nucleic Acid Chem* (9):12.2.1–12.2.12.